J. Appl. Cryst. (1994). **27**, 463–474

Approximate Intensity Solutions for the Multiple Diffraction of Neutrons in a Many-Beam Case

BY C. B. R. PARENTE, V. L. MAZZOCCHI AND F. J. F. PIMENTEL*

Instituto de Pesquisas Energéticas e Nucleares, Comissão Nacional de Energia Nuclear, CP 11049 - *Pinheiros*, 05422-970 - *São Paulo, SP, Brazil*

(*Received* 3 *July* 1992; *accepted* 18 *August* 1993)

Abstract

Based on the theory developed for the multiple diffraction of neutrons in mosaic crystals, approximate intensity solutions have been derived allowing the calculation of multiple diffraction intensities when several ($n \geq 4$) beams contribute to the phenomenon. The solutions are also appropriate for the calculation of intensities when high absorption and high secondary extinction are present. From these solutions, a computer program (*MULTI*) has been written in order to simulate neutron multiple diffraction patterns. A brief description of *MULTI* and an example of its application to the simulation of high-secondary-extinction/high-density neutron multiple diffraction patterns are included.

1. Introduction

Since Renninger (1937) first made a complete experimental study of the X-ray multiple diffraction in diamond and rock salt, there has been a progressive increase in the number of articles dealing with this phenomenon. A few of them deal with the development of adequate theories for the multiple diffraction of X-rays, neutrons or electrons, using either the dynamical theory or the kinematical theory of diffraction. In a recent book, Chang (1984) focused attention on X-ray multiple diffraction and its application in crystallographic studies and gave an overall review of these theories. Particular attention is given to the intensity solutions derived for both theories. Chang's book is, in fact, a useful survey of those articles dealing with intensity calculations in multiple diffraction prior to 1984. Recently, Soejima, Okazaki & Matsumoto (1985) used the kinematical theory developed for the multiple diffraction (m.d.) of X-rays and neutrons to write a computer program for the simulation of m.d. patterns obtained with φ and λ scans. They applied the program to some experimental X-ray and neutron φ-scan data already available in the literature and found that the calculated patterns were in very good agreement with the experimental ones. As pointed out by these authors, the quality of the agreement shows the validity of the kinematical theory when applied to m.d. intensity calculations. More recently, Rossmanith (1986) also applied the kinematical theory to the calculation of *Umweganregung* patterns (hereafter shortened to *Umweg* patterns). The author calculated *Umweg* patterns for the forbidden 00.3 reflection of zinc using the wavelengths of Cu $K\alpha_1$ and Cu $K\alpha_2$ radiation and compared them with the experimental φ scan obtained with Cu $K\alpha$ radiation. An excellent agreement between measured and calculated intensities is reported when Lorentz factors for the scans involved in the measurements (θ and φ scans) are taken into account. It should be mentioned that, in both studies referred to above, intensity calculations for higher-order diffraction ($n \geq 4$; in this work called a many-beam case) were carried out by considering only three-beam interactions. In other words, the intensity of an n-beam interaction was approximated by summing the effects of the three-beam interactions formed by the incident, primary and each of the secondary beams. However, this approximation disregards entirely the interactions between secondary beams although these interactions involve, in general, reflection coefficients (reflectivities) of the same order of magnitude as those involved in a three-beam interaction. Therefore, it is reasonable to conclude that, in order to ensure a better approximation, interactions between secondary beams cannot be neglected in the intensity calculations.

In this work, approximate intensity solutions appropriate for a many-beam case are derived. The recurrence formula (Parente & Caticha-Ellis, 1974*a*) was employed in the derivations in order to allow intensity calculations when high absorption and high secondary extinction are present. *MULTI*, a computer program for the simulation of m.d. patterns which uses the solutions derived in this work, has been written and applied in a study of the β-quartz structure employing neutron multiple diffraction as a method of analysis (Mazzocchi & Parente, 1994). The

* Present address: Max-Planck-Institut für Metallforschung, Institut für Werkstoffwissenschaft, D-7000 Stuttgart, Germany.

program and an example of its application to a m.d. pattern are briefly presented in §6.

2. Basic theory

In 1964, Moon & Shull presented a theory for the multiple diffraction of neutrons in a mosaic crystal having the shape of a flat plate large compared to the incident-beam cross section. This theory is an extension of the kinematical treatment of the secondary extinction developed for the (single) neutron diffraction in mosaic crystals (see, for example, Bacon & Lowde, 1948). Primary extinction is assumed to be negligible.

Moon & Shull's differential equations, describing the change in power in the several beams traversing a layer of thickness dx at depth x below the surface of a crystal plate, can be written in the following concise form (Parente & Caticha-Ellis, 1974*a*):

$$P_i^{(1)}(x) = s_i \sum_{j \neq i} [P_j(x)/\gamma_j]\bar{Q}_{ji} - s_i P_i(x)(A_i/\gamma_i), \quad (1)$$

where

$$P_i^{(1)}(x) = dP_i(x)/dx$$

$$s_i = \begin{cases} +1 & \text{for transmitted beams} \\ -1 & \text{for reflected beams} \end{cases}$$

and

$$A_i = \mu + \sum_{j \neq i} \bar{Q}_{ij}.$$

Symbols P_i, P_j, s_i, μ, $\bar{Q}_{ij}$ and γ_i are, respectively, the power in beam i, the power in a beam $j \neq i$, the sign of beam i characterizing its type (as above), the linear absorption coefficient, the linear reflection coefficient, or reflectivity, for the exchange of power from beam i to beam j and the magnitude of the direction cosine of beam i relative to the normal to the crystal surface. Subscripts i and j refer to all beams involved in the phenomenon including incident and primary beams.

According to Moon & Shull (1964), the reflectivity for an interaction $i \rightarrow j$ is given by

$$r_{ij} = Q_{ij} W(\Delta\theta_{ij}),$$

where Q_{ij} is the integrated reflectivity per unit volume of a small crystallite and $W(\Delta\theta_{ij})$ is the mosaic distribution function, where $\Delta\theta_{ij}$ is the deviation in the Bragg angle θ_{ij} from the mean of the distribution. The usual expressions for Q and W found in the literature are valid only for a particular rotation of the reflecting planes, as occur in the normal-beam equatorial method. In such a method, the reflecting planes are parallel to the rotation axis, which is perpendicular to both incident and diffracted beams. Zachariasen (1945), in the development of his theory of X-ray diffraction in crystals, derived an integrated-intensity formula for the rotating-crystal method. Zachariasen generalized assuming an arbitrary rotation of the diffracting planes around an axis forming a constant angle with the incident beam. In particular, in a m.d. experiment, the crystal rotates around the scattering vector of the primary reflection and the planes producing secondary reflections make arbitrary rotations around this vector. The rotation around the scattering vector defines the azimuthal angle φ, which is the angle an arbitrary crystallographic direction, lying on a plane perpendicular to the scattering vector of the primary reflection, makes with the projection of the direction of the primary beam on the same plane. In order to take into account the arbitrary rotations of the secondary planes, Moon & Shull (1964) used Zachariasen's integrated formula to write Q for the neutron m.d. case:

$$Q'_{ij} = Q_{ij}/K^{\varepsilon}_{ij} = (\lambda^3 N_c^2 F_{ij}^2/\sin 2\theta_{ij})(1/K^{\varepsilon}_{ij}),$$

where λ is the neutron wavelength, N_c is the number of unit cells per unit volume, F_{ij} and θ_{ij} are, respectively, the structure factor and the Bragg angle for the reflection $i \rightarrow j$, *i.e.* for the reflection by crystallographic planes with Miller indices given by $h_j - h_i$, $k_j - k_i$, $l_j - l_i$. K^{ε}_{ij} is a geometric factor relating $\Delta\theta_{ij}$ and $\Delta\varepsilon$, the latter being an angular deviation due to a rotation around an arbitrary axis ε. In terms of a m.d. experiment, ε is aligned with the scattering vector of the primary reflection and $\Delta\varepsilon$ corresponds to the deviation in the azimuthal angle φ from the position where the interaction $i \rightarrow j$ is maximum. The relationship between $\Delta\theta_{ij}$ and $\Delta\varepsilon$ is given by (Moon & Shull, 1964)

$$\Delta\theta_{ij} = [(\sin \Phi \cos X \cos \xi)_{ij}/\sin 2\theta_{ij}]\Delta\varepsilon = K^{\varepsilon}_{ij}\Delta\varepsilon,$$

where X is the angle formed by the direction of beam i and its projection on the plane perpendicular to the rotation axis ε, ξ is the angle equivalent to X for the beam j and Φ is the angle between the two projections. $W(\Delta\theta_{ij})$ is, in general, assumed to have a Gaussian form. In terms of the rotation ε, the Gaussian distribution renormalized to unity is given by

$$W(\Delta\varepsilon) = [K^{\varepsilon}_{ij}/(2\pi)^{1/2}\eta] \exp[-(K^{\varepsilon}_{ij}\Delta\varepsilon)^2/2\eta^2],$$

where η is the mosaic spread of the crystal. Reflectivities r_{ij}, but using the symbol $\bar{Q}_{ij}$ as in (1), may then be written as (Moon & Shull, 1964)

$$\bar{Q}_{ij} = Q'_{ij} W(\Delta\varepsilon)$$
$$= [\lambda^3 N_c^2 F_{ij}^2/\sin 2\theta_{ij}(2\pi)^{1/2}\eta] \exp[-(K^{\varepsilon}_{ij}\Delta\varepsilon)^2/2\eta^2].$$

Moon & Shull proposed a Taylor-series expansion of $P_1(x)$ about the point $x = 0$ as a useful approximate solution for the intensity of the primary beam. They derived an analytical formula for the expansion retaining terms up to second order. As

pointed out in their work, the formula is valid only in the limits of low secondary extinction and low absorption. Caticha-Ellis (1969) derived the exact solution for the double- and triple-beam cases. He also derived a second-order approximation for the many-beam case and a third-order approximation for the triple-beam case. However, even with a third-order approximation, intensity calculations were limited to low secondary extinction and low absorption. Obviously, the exact solution can be applied in any situation of extinction and absorption. However, its limitation to a triple-beam case is a shortcoming. On the other hand, derivation of an exact solution for the many-beam case seems to be a formidable task owing to the multitude of cases concerning number and type of beams. The same can be said for the derivation of analytical formulas for higher-order approximations. In order to apply the more convenient Moon & Shull approximate solutions, Parente & Caticha-Ellis (1974*a*) derived a recurrence formula for the summation of the Taylor-series expansion up to any desired order m. In the formulation presented by the authors, the expansion, generalized for any beam i, can be written

$$P_i(x) = P_i(0) + P_i^{(1)}(0)x + P_i^{(2)}(0)x^2/2! + \ldots + P_i^{(m)}(0)x^m/m! + \ldots, \quad (2)$$

where the general term is given by

$$(1/m!)x^m P_i^{(m)}(0) = (1/m!) \sum_k P_k(0) Y_{ki}^{(m)}. \quad (3)$$

In the general term, $P_i^{(m)}(0)$ is the mth derivative of the power $P_i(x)$ calculated at $x = 0$, *i.e.*

$$P_i^{(m)}(0) = \mathrm{d}^m P_i(x)/\mathrm{d}x^m|_{x=0},$$

$P_k(0)$ is the power of a beam k at the point $x = 0$ and the coefficient* $Y_{ki}^{(m)}$ is calculated from the coefficient of order $(m-1)$ by

$$Y_{ki}^{(m)} = \sum_j X_{kj} Y_{ji}^{(m-1)}, \quad (4)$$

where

$$X_{kj} = s_j \bar{Q}_{kj} x/\gamma_k \qquad \text{for } k \neq j$$

and

$$X_{jj} = -s_j A_j x/\gamma_j \qquad \text{for } k = j.$$

The ratio $x/\gamma_i = l_i$ corresponds to the effective path length of a beam i traversing a crystal layer of thickness x in an infinite crystal plate of thickness T. In general, the total power in beam i is required. In such a case, x is made equal to the plate thickness T, as shown in the solutions derived in the next section. In a thick plate, effective path lengths can be limited by absorption. This is particularly true in the X-ray case (Caticha-Ellis, 1969). With neutrons, however, absorption is generally negligible and effective path lengths are limited by the plate thickness unless beams are parallel to its faces. Therefore, for a crystal plate with negligible absorption, $l_i = T/\gamma_i$, $\gamma_i \neq 0$. If a beam is parallel or makes a small angle with the crystal faces, *i.e.* if $\gamma_i \simeq 0$, l_i is either dependent on the dimensions of the faces or on the absorption. For a different crystal shape or even for a plate that cannot be considered as satisfying the above conditions, path lengths are defined, in general, by taking into account all dimensions of the crystal (Parente & Caticha-Ellis, 1974*a*).

Equation (4) is the recurrence formula that allows the calculation of the successive terms of the Taylor-series expansion in an iterative way, *i.e.* the mth-order term is calculated as soon as the $(m-1)$th term is obtained. As is implicit in the above formulation, the diffracted beams involved in the phenomenon can be of any type in any number. The coefficients for the first-order term $(m = 1)$ are calculated from the coefficients of the zero-order term defined by

$$Y_{ki}^{(0)} = \begin{cases} 0 & \text{for } k \neq i \\ 1 & \text{for } k = i. \end{cases} \quad (5)$$

The summation of the successive terms in (2), obtained by calculating iteratively the general term (3) to any desired order, gives the approximate intensity solution $P_i(x)$ for the beam i. Provided a computer is used, approximations with hundreds of terms can be calculated using the recurrence formula. It should be mentioned at this point that, even for a case involving high secondary extinction and/or high absorption, a good approximation can be attained, in general, with a few tens of terms. An example is found in the work by Parente & Caticha-Ellis (1974*b*), where the 111 primary intensity of aluminium was measured with a single crystal in the shape of a square plate $3 \times 3 \times 1$ in oriented with the (111) planes parallel to the 3×3 in face. Using the recurrence formula, the authors calculated intensities in four different interaction cases and compared them with experimental results. In spite of the quite high secondary extinction present in the measured intensities, a maximum of 14 terms was more than enough to obtain a good approximation in the four cases considered in the work.

Based on the theory outlined above, intensity solutions appropriate for a many-beam case are derived in the next section. Owing to the employment of the recurrence formula in the derivation, the solutions are also appropriate in cases involving high secondary extinction and/or high absorption.

* In the original formulation, the symbol used is ${}^{(m)}X_{ki}$. To avoid confusion with the symbol X_{ki}, it is substituted here by $Y_{ki}^{(m)}$. Equation (3) includes the numerical factor $1/m!$, which is omitted in the original equation.

3. Approximate intensity solutions for a many-beam case

In this section, approximate intensity solutions are derived by using the general term of the Taylor-series expansion in the case of n beams diffracted in a crystal plate of thickness T.

Expansion (2) written for $x = T$ becomes

$$P_i(T) = P_i(0) + P_i^{(1)}(0)T + P_i^{(2)}(0)T^2/2! + \ldots + P_i^{(m)}(0)T^m/m! + \ldots. \quad (6)$$

To find the terms of expansion (6), use is made of (3) and (4) obtaining, after appropriate algebraic manipulations and simplifications,

$$\begin{aligned} R_i' = {} & R_0(Y_{0i}^{(1)} + Y_{0i}^{(2)}/2! + \ldots + Y_{0i}^{(m)}/m! + \ldots) \\ & + R_1(Y_{1i}^{(1)} + Y_{1i}^{(2)}/2! + \ldots + Y_{1i}^{(m)}/m! + \ldots) \\ & + R_2(Y_{2i}^{(1)} + Y_{2i}^{(2)}/2! + \ldots + Y_{2i}^{(m)}/m! + \ldots) + \ldots \\ & + R_i(1 + Y_{ii}^{(1)} + Y_{ii}^{(2)}/2! + \ldots + Y_{ii}^{(m)}/m! + \ldots) \\ & + \ldots + R_{(n-1)}(Y_{(n-1)i}^{(1)} + Y_{(n-1)i}^{(2)}/2! + \ldots \\ & + Y_{(n-1)i}^{(m)}/m! + \ldots), \end{aligned} \quad (7)$$

where $R_i' = P_i(T)/P_0(0)$ and $R_i = P_i(0)/P_0(0)$. In (7), indices 0 and 1 indicate, respectively, the incident beam and the primary beam; other indices indicate secondary beams. $P_0(0)$ is the power of the incident beam, which is, of course, different from zero, and, in general, not precisely known. For this reason, both members of (7) were divided by $P_0(0)$. Obviously, $R_0 = 1$. For further simplification, the coefficients of the power ratios R in (7) can be represented by

$$\sum_m Y_{ji}^{(m)}/m! = C_{ji} \quad \text{for } j \neq i$$

and

$$1 + \sum_m Y_{ii}^{(m)}/m! = C_{ii} \quad \text{for } j = i$$

and (7) rewritten as

$$R_i' = C_{0i}R_0 + C_{1i}R_1 + C_{2i}R_2 + \ldots + C_{ii}R_i + \ldots + C_{(n-1)i}R_{(n-1)}, \quad (7a)$$

where $C_{0i}, C_{1i}, \ldots, C_{ii}, \ldots, C_{(n-1)i}$ can be determined from (4) iteratively.

To solve (7a), it is necessary to apply the boundary conditions for the diffraction powers of the beams involved, including the beam i itself. These boundary conditions at the entrance ($x = 0$) and exit ($x = T$) surfaces of the crystal plate are, according to Caticha-Ellis (1969) and in terms of the ratios R_j,

$$\begin{aligned} & R_j \neq 0 \quad \text{and} \quad R_j' = 0, \quad \text{when } j \text{ is a reflected beam;} \\ & R_j = 0 \quad \text{and} \quad R_j' \neq 0, \quad \text{when } j \text{ is a transmitted beam.} \end{aligned} \quad (8)$$

Applying the boundary conditions (8) exclusively for the beam i, (7a) is reduced to one of the following equations:

$$R_i = -\left(\sum_{\substack{j=0 \\ j\neq i}}^{n-1} R_j C_{ji}\right) \Big/ C_{ii} \quad \text{for a beam } i \text{ reflected} \quad (9)$$

$$R_i' = \sum_{\substack{j=0 \\ j\neq i}}^{n-1} R_j C_{ji} \quad \text{for a beam } i \text{ transmitted.} \quad (10)$$

When using (9) or (10) to calculate the intensity of a beam i, the application of the boundary conditions must be extended to the other beams. Power ratios R_j corresponding to transmitted beams are made zero. Nevertheless, they contribute to the power of beam i through the coefficients C_{ji}, C_{ii} included. It should be noted that, although the incident beam ($j = 0$) is always a transmitted beam, as mentioned before, $R_0 = 1$. Because of this, the restriction $j \neq i$ disappears if (10) is used to calculate the intensity of the incident (transmitted) beam.

Power ratios R_j corresponding to reflected beams can be determined from (9). A set of linear equations, with a maximum of $n - 2$ equations, is then obtained. The system formed by the equations can be represented in a matrix form by

$$\begin{pmatrix} C_{11} & C_{21} & \ldots & C_{(n-1)1} \\ C_{12} & C_{22} & \ldots & C_{(n-1)2} \\ \vdots & \vdots & & \vdots \\ C_{1(i-1)} & C_{2(i-1)} & \ldots & C_{(n-1)(i-1)} \\ C_{1(i+1)} & C_{2(i+1)} & \ldots & C_{(n-1)(i+1)} \\ \vdots & \vdots & & \vdots \\ C_{1(n-1)} & C_{2(n-1)} & \ldots & C_{(n-1)(n-1)} \end{pmatrix} \begin{pmatrix} R_1 \\ R_2 \\ \vdots \\ R_{(i-1)} \\ R_{(i+1)} \\ \vdots \\ R_{(n-1)} \end{pmatrix} = -\begin{pmatrix} C_{01} \\ C_{02} \\ \vdots \\ C_{0(i-1)} \\ C_{0(i+1)} \\ \vdots \\ C_{0(n-1)} \end{pmatrix}. \quad (11)$$

System (11) can easily be solved if the number of equations is small. For a large number, one of several suitable subroutines available in computer libraries can be used. Finally, substituting the R_j's found by solving (11) in the appropriate equation, (9) or (10), the approximate solution sought is then obtained.

4. About the linear reflectivity coefficients

As seen in §2, the transfer of power between any two beams i and j depends on the linear reflectivity $\bar{Q}_{ij}$, which is a function of $\Delta\theta_{ij}$, the deviation in the Bragg angle from the mean of the mosaic distribution.

According to the definition of $\Delta\varepsilon$ and its relationship with $\Delta\theta_{ij}$, this latter angular deviation is a function of the azimuthal angle φ. Thus, for a particular interaction $i \rightarrow j$, $\bar{Q}_{ij}$ as a function of φ increases from zero to a maximum occurring at an angle corresponding to the point where the maximum of the mosaic distribution touches the Ewald sphere. After this point, the reflectivity decreases from the maximum to zero. According to the definition of $\bar{Q}_{ij}$ in §2, a reflectivity curve has the same form as the mosaic distribution function. Its width, although enlarged by the effect of the geometrical factor, is of the same order of magnitude as the mosaic spread of the crystal, in general a few tenths of a degree. Therefore, for a high-density m.d. pattern, where secondary reflections occur with a narrow spacing between them, all reflections in the neighborhood of a certain value of φ contribute to the intensity at that point. Fig. 1 shows a few linear reflectivity curves obtained from the output data of *MULTI* during the calculation of intensities in the previously mentioned study of β-quartz. A Gaussian mosaic distribution was assumed in the calculations. The reflectivity curves correspond to the interactions between a secondary beam labeled 2 and its neighbors in a particular interval of φ. The interactions also include incident and primary beams labeled 0 and 1, respectively. Correspondence between labels and actual reflections in the β-quartz study is as follows: label 1: 00.1 reflection; label 2: $\bar{2}2.0$; label 3: $\bar{2}2.1$; label 4: $\bar{1}6.\bar{3}$; label 5: $\bar{1}6.4$; label 6: $41.\bar{3}$; label 7: 41.4. For the sake of clearness in the drawing, the $\bar{Q}$ scale was made logarithmic and some curves were not completely traced. The logarithmic scale precludes that the reflectivity curves have the usual Gaussian form. Neverthess, a better distinction between them is possible, particularly in the region where the values of $\bar{Q}$ are very small. As an illustration of the observations made above, the values assumed by the reflectivities $\bar{Q}_{2j}$ and $\bar{Q}_{j2}$ at an arbitrary φ, namely 45.2°, correspond to the points of the intersection of the curves with the vertical dashed line. Actually, more than the 12 values shown in the figure must be considered in the intensity calculations at that point. In fact, each of the eight beams in the example interacts with its seven neighbors. For n beams, $n(n-1)$ interactions occur. This gives 56 interactions for the case partially shown in the figure. Of course, an interaction can be neglected if either its reflectivity has no significant value at the φ considered or the interaction itself corresponds to a forbidden reflection. In Fig. 1, reflectivities $\bar{Q}_{26}$ and $\bar{Q}_{27}$ correspond to the former case since, at $\varphi = 45.2°$, they are a factor of about 10^{-6} and 10^{-4}, respectively, smaller than the reflectivity $\bar{Q}_{21}$, the highest one. Interactions $2 \rightleftharpoons 3$, on the other hand, correspond to the latter case since reflectivities $\bar{Q}_{23}$ and $\bar{Q}_{32}$ are equal to zero for any value of φ. Obviously, they are not shown in Fig. 1.

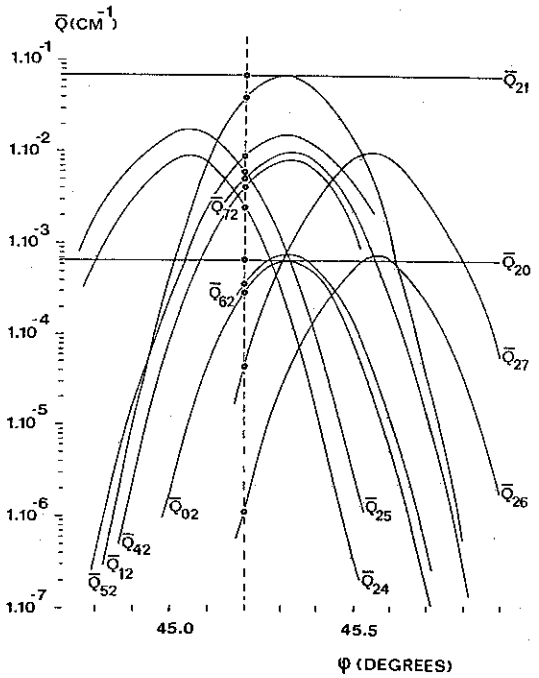

Fig. 1. Reflectivity curves for a real case corresponding to the interactions between a secondary beam, labeled 2, and other beams, labeled 0 (incident), 1 (primary), 4, 5, 6 and 7 (secondaries), occurring in a small interval of φ.

If Friedel's law is valid, the reflectivity for a transfer of power from a beam i to a beam j is the same as that from beam j to beam i, provided both corresponding reciprocal-lattice points traverse the surface of the Ewald sphere at the same time and in the same geometrical conditions. This is true even for a φ value out of the maximum of the m.d. peak or dip. However, if one or both conditions above are not fulfilled, the reflectivity for an interaction $i \rightarrow j$ can be very different from the reverse interaction $j \rightarrow i$. In this situation, for a given φ value, the rate of transfer of power from one beam to another can be very different from the rate of the reverse transfer. In Fig. 1, for instance, reflectivities $\bar{Q}_{21}$ and $\bar{Q}_{12}$, have completely different behaviors. Because the reciprocal-lattice point, RELP, corresponding to the primary reflection is permanently lying on the surface of the Ewald sphere, reflectivity $\bar{Q}_{21}$ is constant and maximum for any value of φ. On the other hand, the RELP corresponding to the secondary reflection traverses the Ewald sphere during the φ-axis rotation and the reflectivity $\bar{Q}_{12}$ varies accordingly reaching a maximum at $\varphi = 45.3°$. Only at this φ value, $\bar{Q}_{21} = \bar{Q}_{12}$; for any other value, $\bar{Q}_{21} > \bar{Q}_{12}$. The same is true for the reflectivities $\bar{Q}_{20}$ and $\bar{Q}_{02}$.

Figs 2(*a*) and (*b*) were prepared to give an explanation for the apparent breakdown of Friedel's law mentioned above for the reflectivities $\bar{Q}_{20}$ and

$\bar{Q}_{02'}$. They are schematic representations of a mosaic crystal in two different angular positions, which result from a rotation around the scattering vector of a primary reflection. In the upper part of each figure, a simplified two-dimensional view of the reciprocal space shows the Ewald sphere associated with the incident beam, a RELP 0 corresponding to the origin of the reciprocal lattice of the crystal and a RELP 2 capable of producing a secondary reflection. It is assumed that the reciprocal-lattice vector for the primary reflection $\mathbf{H}_{01}$ is perpendicular to the figures through RELP 0. For the sake of clearness of drawing, RELP 1, $\mathbf{H}_{01}$ and $\mathbf{H}_{10}$ are not indicated in this part of the figures. It should be noted that RELPs 0 and 1 lie permanently on the surface of the sphere, no matter what the rotation. This is a previous condition for the systematic occurrence of multiple diffraction peaks or dips in a Renninger scan (Renninger, 1937). In Fig. 2(*a*), RELP 2 is close enough to the Ewald sphere to allow the mosaic distribution to touch its surface. This is represented by small circles concentric with RELP 2 intercepting the surface at a level indicated by the dashed circumference. Point 2′ is a RELP in the intersection at the correct distance from RELP 0 to make interactions $0 \rightleftharpoons 2'$ effective. $\mathbf{H}_{02'}$ and $\mathbf{H}_{2'0}$ are the corresponding reciprocal-lattice vectors; $\mathbf{k}_0$ and $\mathbf{k}_{2'}$ are the wave vectors along the incident and secondary beams, respectively. In Fig. 2(*b*), the maximum of the mosaic distribution intercepts the surface of the sphere. Consequently, RELP 2 is in the position previously occupied by RELP 2′. Reciprocal-lattice and wave vectors corresponding to the interactions $0 \rightleftharpoons 2$ are indicated in the figure.

In the lower parts of Fig. 2, a small region of the mosaic crystal is represented by its individual mosaic blocks. Since the mosaic crystal is oriented to produce the maximum of the primary reflection, the majority of the blocks are in positions to diffract $0 \rightarrow 1$. Such blocks with interactions $0 \rightleftharpoons 1$ are clearly indicated in Fig. 2. In Fig. 2(*a*), the intersection is not in the maximum of the mosaic distribution and only a few blocks exhibit interactions $0 \rightleftharpoons 2'$. It should be noted that 2′ can also be interacting with RELP 1. In such a case, a three-beam interaction occurs. This is also clearly indicated in a few blocks of the figure. Fig. 2(*b*) has a larger number of blocks exhibiting interactions $0 \rightleftharpoons 2$ than Fig. 2(*a*). Of course, this is because the

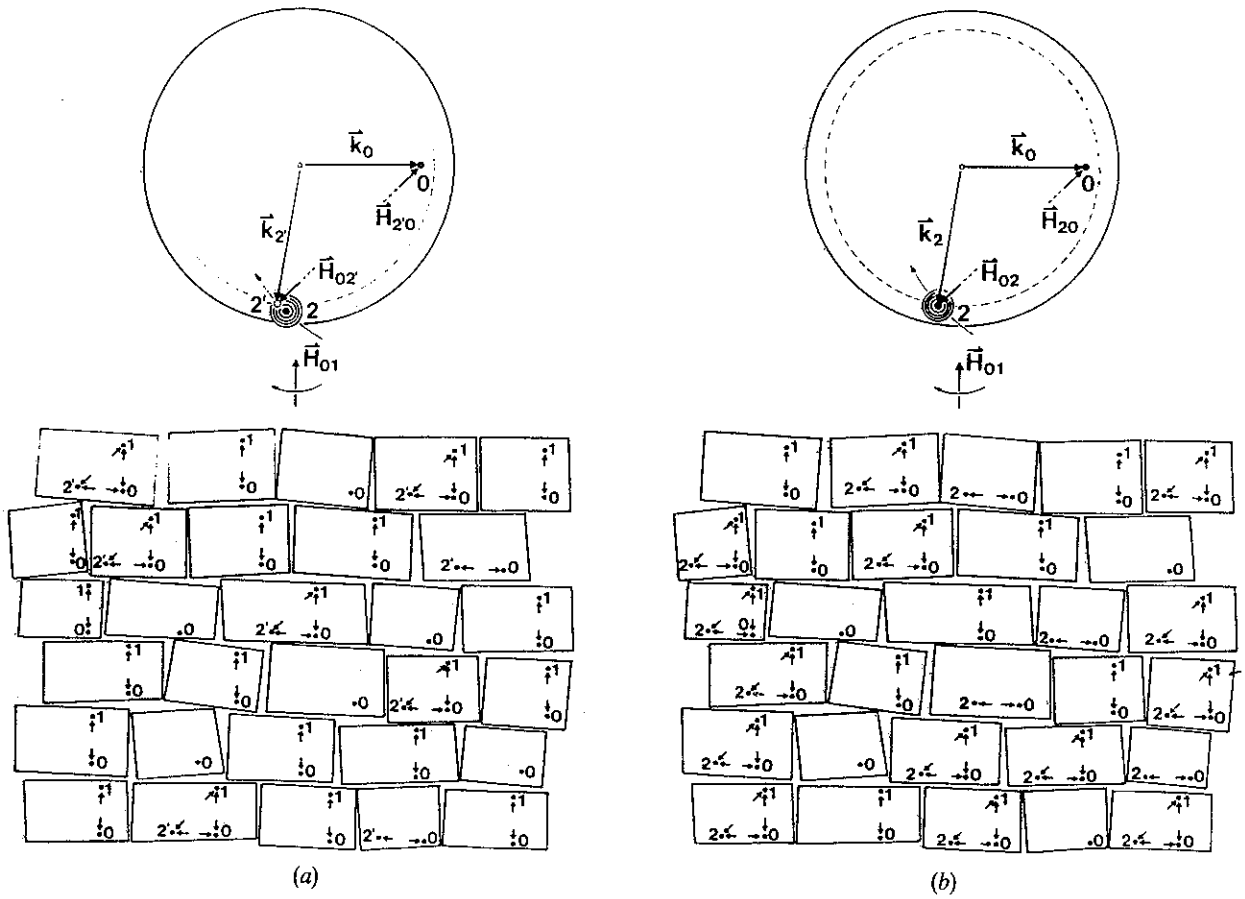

(*a*) (*b*)

Fig. 2. Simplified representations of a mosaic single crystal, in real and reciprocal spaces, in two different azimuthal angular positions, (*a*) and (*b*). They are used in the text to explain an apparent breakdown of Friedel's law expressed by $\bar{Q}_{ij} \neq \bar{Q}_{ji}$.

intersection is in the maximum of the mosaic distribution. Since mosaic blocks are perfect crystals, they individually produce very narrow intrinsic reflection curves. So, a RELP appearing in a certain block of one of the figures will not appear in the same block of the other figure, provided the angular deviation between the two positions is not too small. Obviously, a block containing simultaneously RELPs 0 and 1 is an exception. Such a block is contributing to the intensity of the primary reflection and, as seen before, this condition does not change even in a full turning of the crystal.

With the mosaic blocks regarded as individual perfect single crystals, RELPs 2 and 2′ are the same entity since they are equivalent RELPs in the reciprocal lattices of the blocks. This RELP was labeled differently in the figures only to distinguish points interacting with RELP 0 which are in or out of the maximum of the mosaic distribution. Since there is no need to distinguish this in what follows, RELPs 2 and 2′ are now generalized as RELP 2. The interactions $0 \rightleftharpoons 2$ are split in an obverse direction $0 \rightarrow 2$ and a reverse direction $2 \rightarrow 0$ and a few conclusions can be drawn from a careful observation of the figures. In the reverse direction, the rate of transfer of power is maximum no matter what figure is being observed or, in a more general way, what angular position is assumed by the crystal. This assertion is easily verified by observing that in both figures every block having RELP 2 also has the interaction $2 \rightarrow 0$ occurring. This is the condition used before to define RELP 2. In spite of the fact that the number of such blocks is much less in Fig. 2(*a*) in comparison with Fig. 2(*b*), in both figures all of them are contributing to the interaction in the reverse direction. This makes the rate of transfer of power in such a direction maximum and, moreover, constant. It should be understood that the power transferred in the interaction depends on the strength of the secondary beam. This strength varies as the maximum of the mosaic distribution approaches or leaves the surface of the sphere. The strength of the secondary beam depends on its interaction with all other beams occurring simultaneously. Power is transferred from the secondary to the incident beam at a constant and maximum rate, although the transfer itself varies according to the variation of the secondary-beam strength.

For the obverse direction, the situation is quite different. Most blocks containing RELP 0 also contain RELP 1. Most such blocks remain the same during a crystal rotation. Except for a few occasional occurrences of blocks with RELP 0 without the presence of RELP 1, the number of blocks containing RELP 0 remains unaltered. Then, from observation of Fig. 2(*a*), it is easily verified that, from the total number of blocks containing RELP 0, only a few have interactions $0 \rightarrow 2$ occurring. On the other hand, in Fig. 2(*b*) the number of such blocks is significantly greater than in Fig. 2(*a*). This expresses the fact that the maximum of the mosaic distribution is touching the Ewald sphere. It is easy now to understand why, as opposed to the reverse direction, the rate of transfer of power in the obverse direction varies as the crystal rotates. In such a case, power is transferred from the incident to the secondary beam at a rate which is a function of the position of RELP 2 relative to the surface of the Ewald sphere. The rate of transfer of power has the same form as the mosaic distribution function. It should be noted in Fig. 1 that the maximum value assumed by $\bar{Q}_{02}$ equals $\bar{Q}_{20}$ corresponding to the situation depicted in Fig. 2(*b*). Similarly to the reverse direction, the power transferred to the secondary beam is dependent on the incident-beam strength which, in turn, depends on the several interactions $0 \rightleftharpoons j$ occurring simultaneously.

A somewhat different situation occurs with reflectivities corresponding to interactions between two nonsimultaneous secondary beams such as 2 and 6 in Fig. 1. The reflectivity curve for the interaction $2 \rightarrow 6$ has its maximum at $\varphi = 45.6°$ while for the interaction $6 \rightarrow 2$ the maximum occurs at $\varphi = 45.3°$, although having the same value. For this reason, their reflectivities never assume equal values except when they intersect at an angle halfway between the two maxima. It should be noted that the actual value of φ at the intersection depends on the geometrical factor affecting each curve. It is easily understood that during crystal rotation two RELPs can cross the surface of the Ewald sphere at different inclinations, resulting in different spreads for the curves. Consequently, the intersection occurs at an angle that is not halfway between the two maxima. Only in the case of equal spreads does the intersection occur exactly halfway. Such unusual interactions between secondary beams occur, in general, when they succeed in close sequence in a m.d. pattern, *i.e.* when the pattern exhibits a high density of secondary reflections. It should be mentioned that, even in a low-density m.d. pattern, they are likely to occur in those regions where the density of secondary reflections increases. It is not worthwhile to demonstrate here the above assertions. They could be demonstrated by following similar reasonings to those related to Figs. 2(*a*) and (*b*), provided appropriate modifications are introduced in the figures.

After the comments above, it would seem that $\bar{Q}_{ij}$ never equals $\bar{Q}_{ji}$, except for a few particular values of φ. Certainly this is not true. To have $\bar{Q}_{ij} = \bar{Q}_{ji}$, for any φ value, it is enough that two RELPs corresponding to secondary beams be simultaneous having the same geometrical factor. In this case, only one reflectivity curve represents both reflectivities. No example of this case is seen in Fig. 1.

5. Some applications of the intensity formulas

In this section, the intensity formulas derived in §3 are applied in a few particular n-beam cases recasting some analytical formulas derived in the literature. In the applications, use is made of the recurrence formula (4) and equations (9) or (10), depending on the type of primary beam. Particular attention must be paid to the signs s_i, the values of the zero-order terms (5) defined in §2 and the boundary conditions (8) in §3.

5.1. *Intensity of the primary beam in a second-order approximation when the primary beam and all the secondary beams are transmitted*

Equation (10) must be applied in this case. Since all the secondary beams are transmitted, it is reduced to

$$R_{1,n}^{(2)'} = C_{01} = \sum_{m=1}^{2} Y_{01}^{(m)}/m! = Y_{01}^{(1)} + Y_{01}^{(2)}/2!. \quad (12)$$

In this equation, the first-order term is given by

$$\begin{aligned} Y_{01}^{(1)} &= \sum_{j=0}^{n-1} X_{0j} Y_{j1}^{(0)} \\ &= X_{00} Y_{01}^{(0)} + X_{01} Y_{11}^{(0)} + X_{02} Y_{21}^{(0)} + \dots \\ &\quad + X_{0(n-1)} Y_{(n-1)1}^{(0)} \\ &= X_{01} = \bar{Q}_{01} l_0 \end{aligned} \quad (13)$$

and the second-order term by

$$\begin{aligned} Y_{01}^{(2)} &= \sum_{j=0}^{n-1} X_{0j} Y_{j1}^{(1)} = \sum_{j=0}^{n-1} X_{0j} \left(\sum_{k=0}^{n-1} X_{jk} Y_{k1}^{(0)} \right) \\ &= X_{00}(X_{00} Y_{01}^{(0)} + X_{01} Y_{11}^{(0)} + X_{02} Y_{21}^{(0)} + \dots \\ &\quad + X_{0(n-1)} Y_{(n-1)1}^{(0)}) + X_{01}(X_{10} Y_{01}^{(0)} + X_{11} Y_{11}^{(0)} \\ &\quad + X_{12} Y_{21}^{(0)} + \dots + X_{1(n-1)} Y_{(n-1)1}^{(0)}) \\ &\quad + X_{02}(X_{20} Y_{01}^{(0)} + X_{21} Y_{11}^{(0)} + X_{22} Y_{21}^{(0)} + \dots \\ &\quad + X_{2(n-1)} Y_{(n-1)1}^{(0)}) + \dots + X_{0(n-1)}(X_{(n-1)0} Y_{01}^{(0)} \\ &\quad + X_{(n-1)1} Y_{11}^{(0)} + X_{(n-1)2} Y_{21}^{(0)} + \dots \\ &\quad + X_{(n-1)(n-1)} Y_{(n-1)1}^{(0)}). \end{aligned}$$

From definitions (5) for the zero-order terms, $Y_{01}^{(2)}$ becomes

$$\begin{aligned} Y_{01}^{(2)} &= X_{00} X_{01} + X_{01} X_{11} + \sum_{j=2}^{n-1} X_{0j} X_{j1} \\ &= -A_0 l_0 \bar{Q}_{01} l_0 + \bar{Q}_{01} l_0 (-A_1 l_1) \\ &\quad + \sum_{j=2}^{n-1} \bar{Q}_{0j} l_0 \bar{Q}_{j1} l_j. \end{aligned} \quad (14)$$

Substitution of (13) and (14) into (12) results, after a few manipulations and provided A_0 and A_1 are substituted by their own expressions, in

$$\begin{aligned} R_{1,n}^{(2)'} &= \bar{Q}_{01} l_0 - \tfrac{1}{2} \bar{Q}_{01} l_0 \Big[\mu l_0 + \mu 1_1 + \bar{Q}_{01} l_0 \\ &\quad + \bar{Q}_{10} l_1 + \sum_{j=2}^{n-1} (\bar{Q}_{0j} l_0 + \bar{Q}_{1j} l_1) \Big] \\ &\quad + \tfrac{1}{2} \sum_{j=2}^{n-1} \bar{Q}_{0j} l_0 \bar{Q}_{j1} l_j. \end{aligned} \quad (15)$$

Regardless of the different symbols used, (15) above is identical with (7) derived by Moon & Shull (1964) for the same case.

5.2. *Intensity of the primary beam in a second-order approximation when the primary beam is reflected and all the secondary beams are transmitted*

Equation (9) must be applied now. Similar to the first case (§5.1), it is reduced to

$$R_{1,n}^{(2)} = -C_{01}/C_{11}. \quad (16)$$

C_{01} can be deduced in a straightforward manner observing that it differs from C_{01} in (15) only by the sign s_1, which is now equal to -1. Then, using appropriate symbols for this case, C_{01} can be written

$$\begin{aligned} C_{01} &= -\bar{Q}_{01} l_0 + \tfrac{1}{2} \bar{Q}_{01} l_0 (A_0 l_0 - A_1 l_1) \\ &\quad - \tfrac{1}{2} \sum_{j=2}^{n-1} \bar{Q}_{0j} l_0 \bar{Q}_{j1} l_j. \end{aligned}$$

On the other hand, C_{11} can be calculated by

$$C_{11} = 1 + \sum_{m=1}^{2} Y_{11}^{(m)}/m! = 1 + Y_{11}^{(1)} + Y_{11}^{(2)}/2!,$$

where

$$Y_{11}^{(1)} = \sum_{j=0}^{n-1} X_{1j} Y_{j1}^{(0)} = X_{11} = A_1 l_1$$

and

$$\begin{aligned} Y_{11}^{(2)} &= \sum_{j=0}^{n-1} X_{1j} Y_{j1}^{(1)} \\ &= X_{10} Y_{01}^{(1)} + X_{11} Y_{11}^{(1)} + \sum_{j=2}^{n-1} X_{1j} Y_{j1}^{(1)} \\ &= X_{10} Y_{01}^{(1)} + X_{11} Y_{11}^{(1)} + \sum_{j=2}^{n-1} X_{1j} \left(\sum_{k=0}^{n-1} X_{jk} Y_{k1}^{(0)} \right). \end{aligned}$$

$Y_{01}^{(1)}$ in the first term of the summation is given by (13) in the preceding case. Attention must be paid only to the change in the sign introduced by s_1. $Y_{11}^{(1)}$, in the

second term, can be found above as the second term in C_{11}. Then, $Y_{11}^{(2)}$ can be written

$$Y_{11}^{(2)} = X_{10}X_{01} + X_{11}X_{11} + \sum_{j=2}^{n-1} X_{1j}X_{j1}$$

$$= -\bar{Q}_{10}l_1\bar{Q}_{01}l_0 + A_1^2l_1^2 - \sum_{j=2}^{n-1} \bar{Q}_{1j}l_1\bar{Q}_{j1}l_j \qquad (17)$$

and C_{11} becomes

$$C_{11} = 1 + A_1l_1 - \tfrac{1}{2}\left(\bar{Q}_{10}l_1\bar{Q}_{01}l_0 - A_1^2l_1^2 + \sum_{j=2}^{n-1} \bar{Q}_{1j}l_1\bar{Q}_{j1}l_j\right).$$

Finally, substitution of C_{01} and C_{11} in (16) results in

$$R_{1,n}^{(2)} = \bar{Q}_{01}l_0 - \tfrac{1}{2}\bar{Q}_{01}l_0(A_0l_0 - A_1l_1) + \tfrac{1}{2}\sum_{j=2}^{n-1} \bar{Q}_{0j}l_0\bar{Q}_{j1}l_j\left[1 + A_1l_1 - \tfrac{1}{2}\left(\bar{Q}_{10}l_1\bar{Q}_{01}l_0 - A_1^2l_1^2 + \sum_{j=2}^{n-1} \bar{Q}_{1j}l_1\bar{Q}_{j1}l_j\right)\right]^{-1}.$$

For a three-beam case, with $\bar{Q}_{01} = \bar{Q}_{10}$ and $\bar{Q}_{12} = \bar{Q}_{21}$ (see §4), the equation above is reduced to

$$R_{1,3}^{(2)} = \bar{Q}_{01}l_0 - \tfrac{1}{2}\bar{Q}_{01}l_0(A_0l_0 - A_1l_1) + \tfrac{1}{2}\bar{Q}_{02}l_0\bar{Q}_{21}l_2[1 + A_1l_1 - \tfrac{1}{2}(\bar{Q}_{01}^2l_1l_0 - A_1^2l_1^2 + \bar{Q}_{12}^2l_1l_2)]^{-1},$$

which is identical to (17) derived by Caticha-Ellis (1969) for this particular case.

5.3. *Intensity of the primary beam in a third-order approximation when the primary beam is reflected and all the secondary beams are transmitted*

To find the analytical solution $R^{(3)}$ for this case, it is sufficient to add third-order terms to the solution $R_{1,n}^{(2)}$ found in the second case (§5.2). Thus, the coefficient C_{01} is now given by

$$C_{01} = Y_{01}^{(1)} + Y_{01}^{(2)}/2! + Y_{01}^{(3)}/3!,$$

where only $Y_{01}^{(3)}$ has to be obtained. It is given by

$$Y_{01}^{(3)} = \sum_{j=0}^{n-1} X_{0j}Y_{j1}^{(2)}$$

$$= X_{00}Y_{01}^{(2)} + X_{01}Y_{11}^{(2)} + \sum_{j=2}^{n-1} X_{0j}Y_{j1}^{(2)}.$$

In the above summation, $Y_{01}^{(2)}$ and $Y_{11}^{(2)}$ in the first two terms are already given by (14) and (17), respectively. Since the primary beam is reflected in this case, signs in (14) must be appropriately changed. The remaining part of the summation is obtained as follows:

$$\sum_{j=2}^{n-1} X_{0j}Y_{j1}^{(2)} = \sum_{j=2}^{n-1} X_{0j}\left(\sum_{k=0}^{n-1} X_{jk}Y_{k1}^{(1)}\right)$$

$$= \sum_{j=2}^{n-1} X_{0j}\left[\sum_{k=0}^{n-1} X_{jk}\left(\sum_{l=0}^{n-1} X_{kl}Y_{l1}^{(0)}\right)\right]$$

$$= \sum_{j=2}^{n-1} X_{0j}\left(\sum_{k=0}^{n-1} X_{jk}X_{k1}\right)$$

$$= \sum_{j=2}^{n-1} X_{0j}X_{j1}X_{11} + \sum_{j=2}^{n-1} X_{0j}X_{jj}X_{j1} + \sum_{j=2}^{n-1} X_{0j}\left(\sum_{\substack{k=0\\k\neq 1,j}}^{n-1} X_{jk}X_{k1}\right)$$

$$= -A_1l_1\sum_{j=2}^{n-1} \bar{Q}_{0j}l_0\bar{Q}_{j1}l_j + \sum_{j=2}^{n-1} A_jl_j\bar{Q}_{0j}l_0\bar{Q}_{j1}l_j - \sum_{j=2}^{n-1} \bar{Q}_{0j}l_0\left(\sum_{\substack{k=0\\k\neq 1,j}}^{n-1} \bar{Q}_{jk}l_j\bar{Q}_{k1}l_k\right).$$

It is now possible to write $-C_{01}$. For the sake of conciseness, however, this coefficient will be written later on directly as the numerator of $R_{1,n}^{(3)}$. But the denominator C_{11} is obtained in a very similar manner to C_{01}:

$$C_{11} = 1 + Y_{11}^{(1)} + Y_{11}^{(2)}/2! + Y_{11}^{(3)}/3!.$$

As in C_{01}, only the third-order term has to be obtained. It is given by

$$Y_{11}^{(3)} = X_{10}Y_{01}^{(2)} + X_{11}Y_{11}^{(2)} + \sum_{j=2}^{n-1} X_{1j}Y_{j1}^{(2)},$$

where, again, only the remaining part of the summation has to be derived. Following the steps employed in the derivation of the remaining part of $Y_{01}^{(3)}$ results in

$$\sum_{j=2}^{n-1} X_{1j}Y_{j1}^{(2)} = -A_1l_1\sum_{j=2}^{n-1} \bar{Q}_{1j}l_1Q_{j1}l_j + \sum_{j=2}^{n-1} A_jl_j\bar{Q}_{1j}l_1\bar{Q}_{j1}l_j - \sum_{j=2}^{n-1} \bar{Q}_{1j}l_1\left(\sum_{\substack{k=0\\k\neq 1,j}}^{n-1} \bar{Q}_{jk}l_j\bar{Q}_{k1}l_k\right).$$

Finally, the solution can be written

$$R_{1,n}^{(3)} = N_n/D_n,$$

where

$$N_n = \bar{Q}_{01}l_0 + \tfrac{1}{2}\Big[\bar{Q}_{01}l_0(A_1l_1 - A_0l_0) + \sum_{j=2}^{n-1}\bar{Q}_{0j}l_0\bar{Q}_{j1}l_j\Big] + \tfrac{1}{6}\Big[A_0^2l_0^2\bar{Q}_{01}l_0 - A_0l_0A_1l_1\bar{Q}_{01}l_0 - A_0l_0\sum_{j=2}^{n-1}\bar{Q}_{0j}l_0\bar{Q}_{j1}l_j - \bar{Q}_{01}^2l_0^2\bar{Q}_{10}l_1 + A_1^2l_1^2\bar{Q}_{01}l_0 - \bar{Q}_{01}l_0\sum_{j=2}^{n-1}\bar{Q}_{1j}l_1\bar{Q}_{j1}l_j + A_1l_1\sum_{j=2}^{n-1}\bar{Q}_{0j}l_0\bar{Q}_{j1}l_j - \sum_{j=2}^{n-1}A_jl_j\bar{Q}_{0j}l_0\bar{Q}_{j1}l_j + \sum_{j=2}^{n-1}\bar{Q}_{0j}l_0\Big(\sum_{\substack{k=0\\k\neq 1,j}}^{n-1}\bar{Q}_{jk}l_j\bar{Q}_{k1}l_k\Big)\Big]$$

and

$$D_n = 1 + A_1l_1 + \tfrac{1}{2}\Big[-\bar{Q}_{10}l_1\bar{Q}_{01}l_0 + A_1^2l_1^2 - \sum_{j=2}^{n-1}\bar{Q}_{1j}l_1\bar{Q}_{j1}l_j\Big] + \tfrac{1}{6}\Big[\bar{Q}_{01}l_0\bar{Q}_{10}l_1(A_0l_0 - 2A_1l_1) + A_1^3l_1^3 - 2A_1l_1\sum_{j=2}^{n-1}\bar{Q}_{1j}l_1\bar{Q}_{j1}l_j - \bar{Q}_{10}l_1\sum_{j=2}^{n-1}\bar{Q}_{0j}l_0\bar{Q}_{j1}l_j + \sum_{j=2}^{n-1}A_jl_j\bar{Q}_{1j}l_1\bar{Q}_{j1}l_j - \sum_{j=2}^{n-1}\bar{Q}_{1j}l_1\Big(\sum_{\substack{k=0\\k\neq 1,j}}^{n-1}\bar{Q}_{jk}l_j\bar{Q}_{k1}l_k\Big)\Big].$$

A three-beam case where $\bar{Q}_{ij} = \bar{Q}_{ji}$ (see §4) results in

$$R_{1,3}^{(3)} = N_3/D_3,$$

where

$$N_3 = \bar{Q}_{01}l_0 + \tfrac{1}{2}[\bar{Q}_{01}l_0(A_1l_1 - A_0l_0) + \bar{Q}_{02}l_0\bar{Q}_{21}l_2] + \tfrac{1}{6}[A_0^2l_0^2\bar{Q}_{01}l_0 - A_0l_0A_1l_1\bar{Q}_{01}l_0 - A_0l_0\bar{Q}_{02}l_0\bar{Q}_{21}l_2 - \bar{Q}_{01}^3l_0^2l_1 + A_1^2l_1^2\bar{Q}_{01}l_0 - \bar{Q}_{01}l_0\bar{Q}_{12}^2l_1l_2 + A_1l_1\bar{Q}_{02}l_0\bar{Q}_{21}l_2 - A_2l_2\bar{Q}_{02}l_0\bar{Q}_{21}l_2 + \bar{Q}_{02}^2l_0l_2\bar{Q}_{01}l_0)]$$

and

$$D_3 = 1 + A_1l_1 + \tfrac{1}{2}[-\bar{Q}_{01}^2l_0l_1 + A_1^2l_1^2 - \bar{Q}_{12}^2l_1l_2] + \tfrac{1}{6}[\bar{Q}_{01}^2l_0l_1(A_0l_0 - 2A_1l_1) + A_1^3l_1^3 - 2A_1l_1\bar{Q}_{12}^2l_1l_2 - 2\bar{Q}_{02}l_0\bar{Q}_{10}l_1\bar{Q}_{21}l_2 + A_2l_2\bar{Q}_{12}^2l_1l_2].$$

The above formulas are identical* with, respectively, formulas (21) and (21′) derived by Caticha-Ellis (1969) for this particular case.

It should be noted that the solutions $R_{1,n}^{(2)'}$ derived by Moon & Shull (1964), $R_{1,n}^{(2)}$ and $R_{1,n}^{(3)}$ derived here in the second and third cases, respectively, are analytical formulas useful for the calculation of intensities in many-beam cases provided secondary extinction and absorption can be neglected. When using such formulas, or formulas (9) and (10) in a general case, attention must be paid to the differences in the reflectivities pointed out in §4.

6. *MULTI* – a program for the simulation of m.d. patterns

With the intensity solutions derived in §3 and the discussions in §4 taken into account, a computer program, *MULTI*, has been prepared to calculate theoretical m.d. patterns. *MULTI* simulates point-to-point m.d. patterns for primary and transmitted beams. If the primary-beam pattern is of the *Aufhellung* type, either the calculated power or the ratio between the power calculated taking into account the existence of secondary beams and that calculated as if those beams were absent (Caticha-Ellis, 1969) is given as a function of the azimuthal angle φ. The ratio is written as $\Gamma = P_{1,m}/P_{1,s}$, where m and s stand for multiple and single diffraction. For *Umweg* patterns, Γ cannot be defined since $P_{1,s}$ is zero. In this case, *MULTI* directly gives $P_{1,m}$, which is the power variation in the primary beam due to the arising secondary beams. For transmitted beams, the program calculates patterns in the two options above. In this case, $\Gamma = P_{0,m}/P_{0,s}$ where $P_{0,s}$ is always different from zero. The program calculates $P_{1,m}$ and $P_{1,s}$ from (9) or (10), according to the type of beam 1. Equation (10) is used for both $P_{0,m}$ and $P_{0,s}$.

For its application in the study of β-quartz, *MULTI* was modified to simulate m.d. patterns that can be obtained with 00.l primary reflections from a cylindrical quartz crystal oriented with the c axis of the hexagonal cell parallel to the cylinder axis. A brief description of the main features of this version of *MULTI* is given below:

1. For a predetermined 00.l primary reflection, *MULTI* determines all possible secondary reflections occurring in a given interval. This corresponds to the indexing of the pattern. Primary reflection, angular interval of φ and step $\Delta\varphi$ must be specified by the user.

2. It determines the characteristics of the beams, *e.g.* their signs s_i and their mean path lengths l_i. The sign of a beam is determined by verifying if it emerges

* N_3, in this work, and $\mathcal{N}$, in the original solution, differ by the sign in the first third-order triple product, namely $A_0^2l_0^2\bar{Q}_{01}l_0$. As is verified in the derivation of N_3, the sign in this product is +.

from the surface bathed by the incident beam (reflected, $s_i = -1$) or not (transmitted, $s_i = +1$). Its mean path length is calculated in a subroutine written for this purpose.

3. For each φ position, according to the angular interval and step defined by the user, it calculates the reflectivities $\bar{Q}_{ij}$ for all interactions occurring in that position. A matrix of $n(n-1)$ reflectivities is then obtained, n being the number of interacting beams.

4. As mentioned above, *MULTI* calculates the power of the beam, primary or incident, by using (9) or (10). When necessary, the system (11) formed to find the values of $R_j \neq 0$ is solved by the *MA01B* subroutine of the Harwell Subroutine Library (1987), adjoined to *MULTI*. The maximum order for the expansion is specified by the user.

5. *MULTI* gives as output much useful information including, at each φ value, the indices of all reflections involved, the exact value of φ for the maximum of a secondary reflection occurring within the step $\Delta\varphi$ and the power, or the ratio Γ, for the selected beam. It also plots a graph of the calculated pattern.

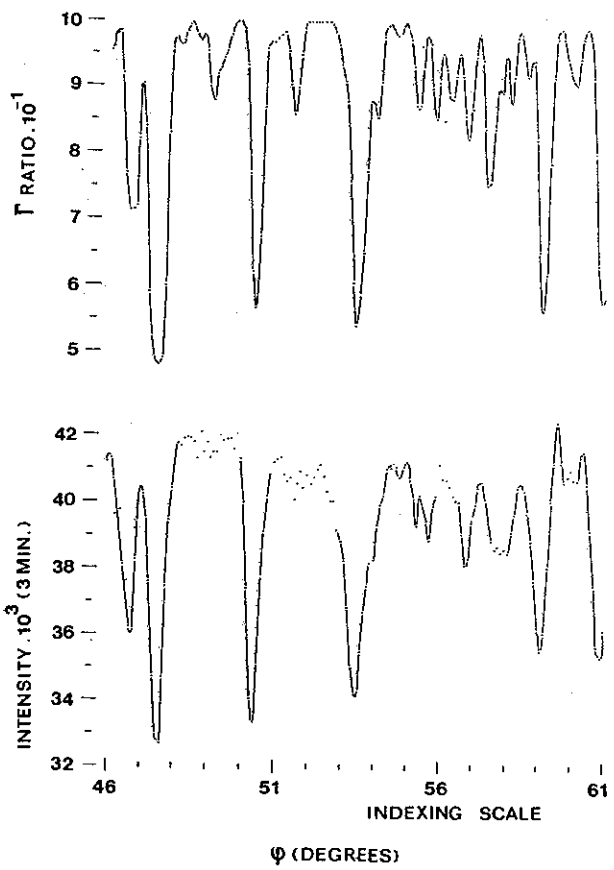

Fig. 3. Comparison between part of the experimental transmitted-beam m.d. pattern of β-quartz and the corresponding simulated pattern calculated by *MULTI* according to a disordered model of the structure.

The application of *MULTI* in the simulation of a m.d. pattern is exemplified in Fig. 3. It shows part of the experimental transmitted beam pattern, obtained concomitantly with the measurement of the 00.1 primary reflection in the study of β-quartz, compared to the corresponding simulated pattern. The experimental pattern was obtained by measuring the incident beam after its passage through the quartz crystal in the β phase. The simulated pattern was calculated by assuming a disordered model of structure. The ratio Γ was calculated instead of the power P_0. Although on different scales, an estimate of the agreement is possible since the greatest peak was made approximately the same height in the two patterns.

A version of *MULTI* for the simulation of X-ray m.d. patterns, *MULTX*, has recently been prepared. An application of this X-ray version to the study of epitaxic layers has been carried out by Salles da Costa, Cardoso, Mazzocchi & Parente (1990).

7. Concluding remarks

The approximate intensity solutions derived in this work allow the calculation of m.d. intensities in many-beam cases, particularly when absorption and secondary extinction are important factors affecting intensities. The correctness of the solutions was verified by applying them in some particular cases, recasting analytical formulas derived in the literature. A computer program, *MULTI*, using these solutions has been written aiming to simulate primary- and transmitted-beam m.d. patterns. In the example of the application of *MULTI* shown in the preceding section, good agreement between calculated and experimental patterns is verified in spite of the high density of secondary reflections and large secondary extinction affecting the experimental pattern.

The authors are indebted to Mrs M. A. H. Trezza for the support given during the implementation of the program *MULTI* on the IBM-4381 computer. They are also indebted to Professor Dr K. Hümmer for a critical reading of the manuscript. One of the authors (VLM) acknowledges the Fundação de Amparo à Pesquisa do Estado de São Paulo (FAPESP) for a fellowship.

References

Bacon, G. E. & Lowde, R. D. (1948). *Acta Cryst.* **1**, 303–314.
Caticha-Ellis, S. (1969). *Acta Cryst.* A**25**, 666–673.
Chang, S.-L. (1984). *Multiple Diffraction of X-rays in Crystals.* Berlin/Heidelberg/New York/Tokyo: Springer-Verlag.

Harwell Subroutine Library (1987). Report AERE 9185, 7th ed. Computer Science and System Division, Harwell Laboratory, Oxfordshire OX11 0RA, England.

MAZZOCCHI, V. L. & PARENTE, C. B. R. (1994). *J. Appl. Cryst.* **27**, 475–481.

MOON, R. M. & SHULL, C. G. (1964). *Acta Cryst.* **17**, 805–812.

PARENTE, C. B. R. & CATICHA-ELLIS, S. (1974*a*). *Jpn. J. Appl. Phys.* **13**, 1501–1505.

PARENTE, C. B. R. & CATICHA-ELLIS, S. (1974*b*). *Jpn. J. Appl. Phys.* **13**, 1506–1513.

RENNINGER, M. (1937). *Z. Phys.* **106**, 141–176.

ROSSMANITH, E. (1986). *Acta Cryst.* A**42**, 344–348.

SALLES DA COSTA, C. A. B., CARDOSO, L. P., MAZZOCCHI, V. L. & PARENTE, C. B. R. (1990). *Defect Control in Semiconductors*, Vol. II, edited by K. SUMINO, pp. 1535–1539. *Proceedings of the International Conference on the Science and Technology of Defect Control in Semiconductors, Yokohama, Japan*, 17–22 *September* 1989. Amsterdam: Elsevier.

SOEJIMA, Y., OKAZAKI, A. & MATSUMOTO, T. (1985). *Acta Cryst.* A**41**, 128–133.

ZACHARIASEN, W. H. (1945). *Theory of X-ray Diffraction in Crystals.* New York: Dover.